© 2021. Published by The Company of Biologists Ltd | Development (2021) 148, dev191619. doi:10.1242/dev.191619

RESEARCH ARTICLE

The atypical RNA-binding protein Taf15 regulates dorsoanterior neural development through diverse mechanisms in *Xenopus tropicalis*

Caitlin S. DeJong[1,*], Darwin S. Dichmann[1,‡], Cameron R. T. Exner[2], Yuxiao Xu[2] and Richard M. Harland[1,§]

ABSTRACT

The FET family of atypical RNA-binding proteins includes Fused in sarcoma (FUS), Ewing's sarcoma (EWS) and the TATA-binding protein-associate factor 15 (TAF15). FET proteins are highly conserved, suggesting specialized requirements for each protein. Fus regulates splicing of transcripts required for mesoderm differentiation and cell adhesion in *Xenopus*, but the roles of Ews and Taf15 remain unknown. Here, we analyze the roles of maternally deposited and zygotically transcribed Taf15, which is essential for the correct development of dorsoanterior neural tissues. By measuring changes in exon usage and transcript abundance from Taf15-depleted embryos, we found that Taf15 may regulate dorsoanterior neural development through *fgfr4* and *ventx2.1*. Taf15 uses distinct mechanisms to downregulate Fgfr4 expression, namely retention of a single intron within *fgfr4* when maternal and zygotic Taf15 is depleted, and reduction in the total *fgfr4* transcript when zygotic Taf15 alone is depleted. The two mechanisms of gene regulation (post-transcriptional versus transcriptional) suggest that Taf15-mediated gene regulation is target and co-factor dependent, contingent on the milieu of factors that are present at different stages of development.

KEY WORDS: Embryo development, FET proteins, Maternal deposition, RNA-seq, Transcript regulation, *Xenopus*

INTRODUCTION

The FET family of atypical RNA-binding proteins includes Fused in sarcoma (FUS), Ewing's sarcoma (EWS) and the TATA-binding protein-associate factor 15 (TAF15). It is a family of heterogeneous nuclear ribonuclear particle (hnRNP) proteins that contain domains for transcriptional activation, and RNA and DNA binding (Schwartz et al., 2015). FET family proteins function in both RNA Polymerase II (RNA Pol II)-mediated transcription and pre-mRNA splicing (Schwartz et al., 2015; Tan and Manley, 2009). Among vertebrates, the three FET members are highly conserved from fish to mammals, suggesting an independent and specialized requirement for each protein (Schwartz et al., 2015). FET proteins have been investigated primarily as components of fusion oncogenes; following abnormal chromosomal translocations, FET protein N-terminal low-complexity/activation domains are found fused to various DNA-binding proteins, contributing to the formation of several cancers (e.g. sarcomas and leukemias) as well as neuronal degenerative diseases (Crozat et al., 1993; Delattre et al., 1992; King et al., 2012; Kovar, 2011; Martini et al., 2002; Neumann et al., 2011; Panagopoulos et al., 1999; Rabbitts et al., 1993; Sjögren et al., 1999; Tan and Manley, 2009; Vance et al., 2009). It has only been more recently that the functions of these proteins have been examined in their full-length 'wild-type' form (Dichmann and Harland, 2012; Schwartz et al., 2015; Tan and Manley, 2009). Studies of the structural, functional and biochemical properties of the FET family proteins determined that these proteins have multiple functions, such that FET proteins may have evolved to facilitate the complex coupling of transcription and mRNA processing that occurs in multicellular organisms (Kato et al., 2012; Schwartz et al., 2015; Schwartz et al., 2013).

The majority of work that has contributed to our understanding of FET protein biology and disease mechanism has been carried out in cell lines and mouse models (Hicks et al., 2000; Li et al., 2007; Scekic-Zahirovic et al., 2016; Sharma et al., 2016; Svetoni et al., 2016; Kapeli et al., 2016), with little known of the role of FET proteins in embryonic development. Previous work from our lab examining the role of Fus in *Xenopus* development found that embryos depleted of Fus exhibit mesoderm differentiation defects and epithelial dissociation (Dichmann and Harland, 2012). The underlying mechanism of these phenotypes was retention of all introns in *fibroblast growth factor 8* (*fgf8*), *fibroblast growth factor receptor 2* (*fgfr2*) and *cadherin 1* (*cdh1*) transcripts (Dichmann and Harland, 2012). Therefore, this study showed that Fus is required for processing of a subset of transcripts in *Xenopus* development. Given the important role of Fus in *Xenopus* development, the perplexing potential for functional redundancy of FET family members in mouse (while remaining highly conserved throughout vertebrates) and the lack of basic research on FET protein functions, we examined the role of Taf15 in early *Xenopus* development, including the role of maternal (M) versus zygotic (Z) Taf15.

To determine the role of Taf15 in early *Xenopus* development, we used RNA-sequencing (RNA-seq) from single embryos depleted of M- and Z-Taf15, using reagents that targeted either all mRNA by inhibiting translation with Morpholino antisense and mismatch oligonucleotides (MOs) or only zygotic function using splice-blocking MOs or CRISPR-mediated mutagenesis. Upon evaluating the transcriptional changes that result from M+Z versus Z-only Taf15 depletion, we found a subset of target genes, the

[1]Molecular and Cell Biology Department, Genetics, Genomics and Development Division, University of California, Berkeley, CA 94720, USA. [2]Department of Psychiatry, Weill Institute for Neurosciences, Quantitative Biosciences Institute, University of California San Francisco, San Francisco, CA 94143, USA.
*Present address: Vaccine and Infectious Disease Division, Fred Hutchinson Cancer Research Center, Seattle, WA 98109, USA. ‡Present address: Invitae Corporation, San Francisco, CA 94103, USA.

§Author for correspondence (harland@berkeley.edu)

C.S.D., 0000-0002-5714-0077; D.S.D., 0000-0001-7994-5442; R.M.H., 0000-0001-8247-4880

Handling Editor: Steve Wilson
Received 15 April 2020; Accepted 8 June 2021

Development (2021) 148, dev191619. doi:10.1242/dev.191619

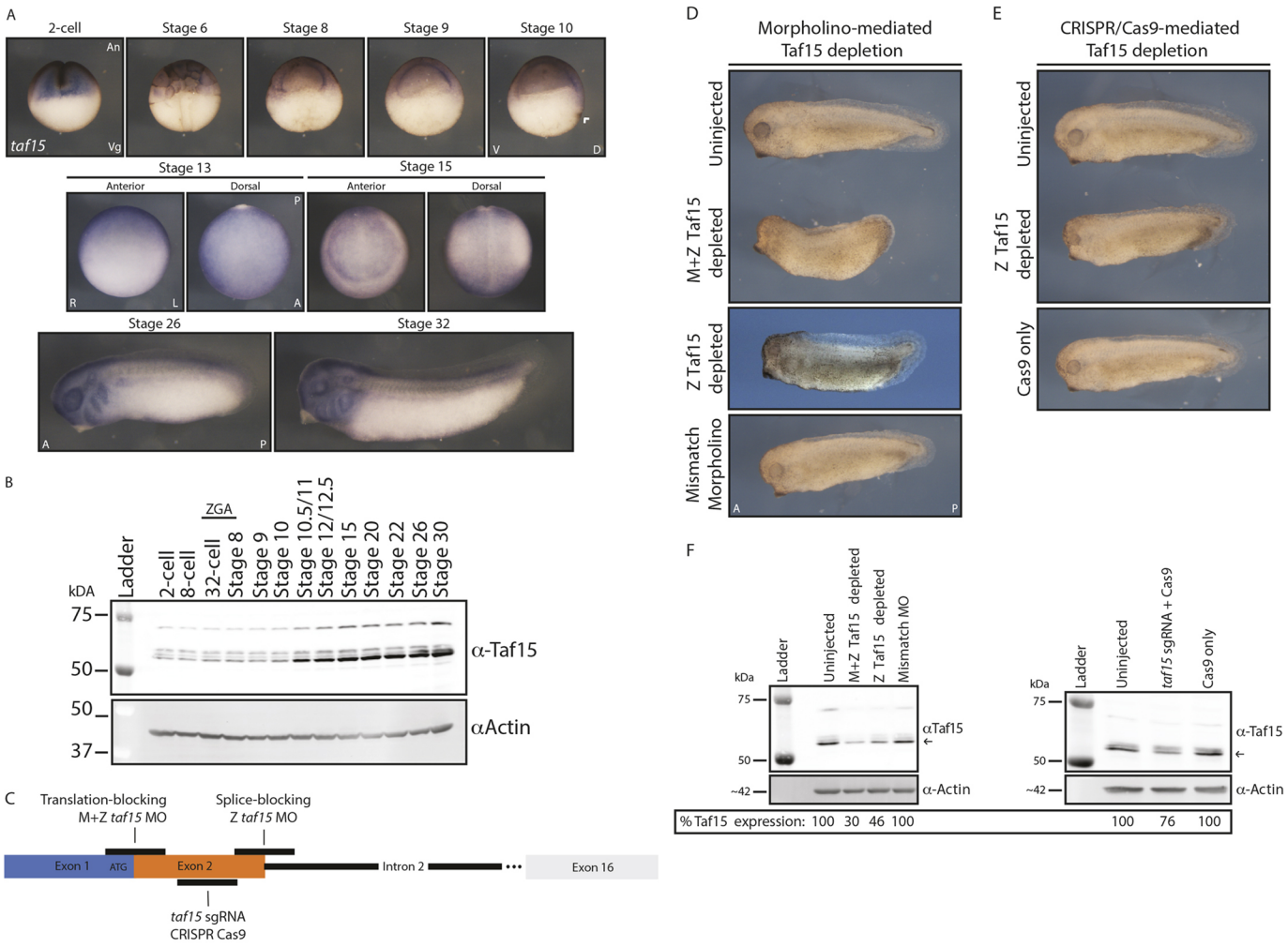

Fig. 1. *taf15*/Taf15 expression and depletion phenotypes. (A) Representative whole-mount ISH of *taf15* transcripts in *Xenopus tropicalis* embryos from the two-cell stage to stage 10. Embryos were cut in half prior to hybridization. White arrowhead indicates the dorsal lip. Images are representative of more than ten embryos. (B) Western blot of Taf15 expression from two-cell-stage embryos through to early tadpoles. (C) Schematic indicating locations of MO and CRISPR/Cas9 target sites. (D) Translation-blocking (M+Z-Taf15 depleted) and splice-blocking (Z-Taf15 depleted) MO-mediated Taf15 depletion. (E) CRISPR/Cas9-mediated Z-Taf15 depletion. Images are representative of more than 12 embryos in D,E. All injections for downstream imaging and western blot analysis were into both cells of two-cell-stage embryos in C,D,E. (F) Representative western blot of Taf15 expression in stage-15 embryos following MO or CRISPR/Cas9-mediated Taf15 depletion. Protein quantification is of the imaged blot using the most consistently expressed Taf15 band marked by the black arrow, normalized to the corresponding Actin band; percentage expression is relative to the uninjected condition; more than three blots were analyzed. A, anterior; An, animal pole; D, dorsal; L, left; P, posterior; R, right; V, ventral; Veg, vegetal pole; ZGA, zygotic genome activation.

expression of which is regulated either post-transcriptionally (via intron retention) or by transcript level, depending on whether M- or Z-Taf15 is depleted. These results suggest that M-Taf15 translation is limiting for splicing of a subset of mRNAs. Furthermore, we show that, during the period of zygotic genome activation (ZGA), zygotic Taf15 modulates the expression of nascent target genes, thus acting at the transcriptional (rather than post-transcriptional) level. Interestingly, we found that, in at least one case that we examined closely, M- and Z-Taf15 have a shared target gene (*fgfr4*), but each acts to regulate *fgfr4* expression through post-transcriptional versus transcriptional mechanisms, respectively. Here, we describe our findings as an example in *Xenopus*, in which the gene product, Taf15, uses distinct molecular mechanisms to regulate the expression of the same gene target (*fgfr4*) depending on the time of development in which Taf15 is expressed (M versus Z) and ensures correct dorsoanterior neural development through two distinct molecular pathways (*fgfr4* and *ventx2.1*).

RESULTS

taf15/Taf15 is both maternally deposited and zygotically transcribed, with a localized expression pattern

To study the role of Taf15 in *Xenopus* development, we first determined the time and place of gene expression at both the transcript and protein level (Fig. 1). From the RNA *in situ* hybridization (ISH) data (Fig. 1A), we observed that *taf15* is enriched in the animal hemisphere throughout the cleavage and gastrula stages (Fig. 1A). During neurulation, *taf15* expression changes from a diffuse dorsal pattern (Fig. 1A, stage 13) to a more specific pattern around the neural plate but still throughout the ectoderm (Fig. 1A, stage 15). Enrichment in the tailbud stage (Fig. 1A, stage 26) occurs in dorsoanterior tissues of the embryo, particularly the brain, branchial arches, anlage of the ear and eye, and pronephros. Lastly, in the early tadpole (Fig. 1A, stage 32), *taf15* is enriched in the central nervous system (anterior and posterior), branchial arches, otic vesicle and the posterior domain of the eye. These data are consistent with protein abundance revealed

Development (2021) 148, dev191619. doi:10.1242/dev.191619

by western blots, which showed that Taf15 is deposited maternally and present throughout embryogenesis, increasing in expression following ZGA (Fig. 1B).

taf15/Taf15 depletion leads to gross morphological defects

To elucidate the role of Taf15 in development, we depleted M+Z-Taf15 protein expression using a translation-blocking MO and Z-Taf15 expression alone using either a splice-blocking MO or CRISPR/Cas9 technology (Fig. 1C-F). Following MO-mediated M+Z-Taf15 depletion, embryos exhibited gross morphological defects, including a shortened anterior-posterior axis, loss of dorsal and posterior fin structures, and reduced eyes and dorsoanterior head structures (Fig. 1D). Not all structures were defective; for example, the cement gland appeared to be unaffected (Fig. 1D). These phenotypes were consistent with the *taf15* expression observed using ISH (Fig. 1A, Stage 32). Although morphological defects were clear in stage-32 tadpoles, early embryos appeared to be relatively normal, although gene expression changes were evident following Taf15 depletion (Figs 2-7). Embryos injected with a translation-blocking MO containing five mismatches to the *taf15* transcript (Mismatch) did not phenocopy the *taf15* morphants, suggesting that the effects of the MO are specific to Taf15 depletion (Fig. 1D). Following Z-Taf15 depletion, by either splice-blocking MO or CRISPR/Cas9 mutagenesis, embryos exhibited a milder phenotype compared with the M+Z-Taf15 depletion, with the most consistent phenotypes between conditions being reduced eyes and dorsoanterior head structures (Fig. 1D,E). Importantly, embryos injected with Cas9 protein alone (Cas9 only) were phenotypically similar to uninjected embryos, again suggesting that the *taf15* short guide (sg)RNA+Cas9 phenotype is specific to the guide that mediates Taf15 depletion (Fig. 1E). The discrepancy in the phenotypes observed following M+Z- or Z-Taf15 depletion suggests some separable developmental roles for M-and Z-Taf15, as explored further below.

To evaluate depletion efficiency, western blot analysis was used to measure total Taf15 following MO or sgRNA+Cas9 injection (Fig. 1F). One possible reason for a milder phenotype following Z-Taf15 depletion is likely the reduced Taf15 depletion efficiency in these conditions compared with M+Z-Taf15 depletion (Fig. 1D-F). Indeed, none of the treatments eliminated Taf15 completely, illustrating the sensitivity of development to the dose of Taf15, confirmed by RNA-seq (see below). Although we attempted to rescue the phenotypes with injected *taf15* mRNA, overexpression was also teratogenic and we were unable to find a dose that gave robust rescue. This is consistent with other experiments in which both increased and decreased expression of splicing regulators induces developmental defects (Dichmann et al., 2008; Iwasaki and Thomsen, 2014). Multiple protein bands (most prominently at ∼55 kDa and ∼60-65 kDa) are observed for Taf15 by western blot (Fig. 1A,E, Fig. 4F). There are two known isoforms of *taf15* in *Xenopus tropicalis*: XM_012956707.2 comprises 1% of the *taf15* transcript and NM_001004806.1 comprises the remaining 99%; all of our depletion tools targeted the latter 99%. Taf15 depletion affected all protein bands, suggesting that they are specific to Taf15 and targets of our depletion tools. As such, we suggest that multiple bands arise from post-translational modifications.

Maternal Taf15 regulates splicing of developmental regulators

In addition to the gross morphological defects that follow Taf15 depletion, changes in gene expression were analyzed by single-embryo RNA-seq. RNA-seq libraries were generated from stage-10 (gastrula stage) and -15 (neurula stage) embryos injected with Taf15 translation-blocking MO (resulting in M+Z-Taf15 depletion) (Fig. 1C, Fig. 2A). The translation-blocking morphants were selected for sequencing because these embryos displayed a more-severe depletion phenotype (Fig. 1D,E) and indicated a consistently more-robust Taf15 depletion (as assayed by western blot; Fig. 1F). Taf15 is a member of the FET family of proteins and the family member Fus is necessary for the correct mRNA splicing of developmental regulators in *Xenopus* (Dichmann and Harland, 2012). To understand how widespread, or conserved, the roles of FET proteins are in splicing regulation in *Xenopus*, we examined changes in intron/exon usage and gene expression levels using the bioconductor packages DEXseq and DESeq, respectively (Love et al., 2014; Reyes et al., 2014) following M+Z-Taf15 depletion (Fig. 2A).

Following DEXseq, a twofold threshold cutoff was applied to the differential exon usage (DEU) gene candidates, followed by PANTHER GO-slim Biological Process analysis. In stage-10 embryos, 228 transcripts were found to exhibit DEU compared with 1429 in stage-15 embryos (Tables S1, S2); 146 and 788 of which were assigned a PANTHER GO-slim Biological Process, respectively (Fig. 2B). For the 100 genes with affected DEU at both stages 10 and 15, termed 'stage persistent' (Table S3), we classified 86 genes with an identified PANTHER GO-slim Biological Process (Fig. 2B). Importantly, because DEXseq measures exon usage, genes with conserved differences in exon usage at both stages 10 and 15 were measured in this stage-persistent DEXseq cohort, rather than an increase or decrease in gene expression. Consistently, we found enrichment for genes involved in cellular and metabolic processes across all stages (Fig. 2B). Using a database designed to differentiate transcripts that are 'maternal', meaning both maternally deposited and zygotically transcribed (i.e. present in the egg and expressed upon ZGA; e.g. *fgfr4*) from 'zygotic' (i.e. transcripts that are exclusively zygotically transcribed; e.g. *isl1*), we compared the percentage of observed target genes with DEUs that have maternal expression to the percentage of all *X. tropicalis* genes with maternal expression (Mitros et al., 2019). The 'observed' category comprised the 100 stage-persistent genes that showed differential exon usage (Table S3) and whether they had M and Z ('maternal') or exclusively Z ('zygotic') transcript expression. We observed that 92% of these stage-persistent DEU target genes had both M and Z transcript expression; the remaining 8% comprised exclusively zygotically expressed genes. The 'expected' category represented the percentage of all annotated *X. tropicalis* genes that had 'maternal' or 'zygotic' transcript expression. Of these *X. tropicalis* transcripts, 65% had both M and Z expression, with the remaining 35% exclusively zygotically expressed (Fig. 2C). Therefore, we were surprised to find 92% of the stage-persistent genes to be transcripts that were both maternally deposited and zygotically transcribed. These data suggest a preference for splice regulation of transcripts that are present throughout development (from egg through ZGA) in this M+Z-Taf15 depletion condition, given that only 65% of annotated *X. tropicalis* transcripts are both maternally deposited and zygotically transcribed (Fig. 2C). Alternatively, it is also possible that intron retention within exclusively zygotic transcripts is less abundant than expected in the M+Z-Taf15-depleted embryos. Interestingly, of the 100 stage-persistent genes, 83 exhibited one-intron retention, 13 had two introns retained and four had more than two introns retained (Fig. 2C). Of the 100 stage-persistent DEU genes, 53 were distributed throughout the top-100 DEU genes of the stage-10 embryo (as sorted by adjusted *P*-values), suggesting that this approach of looking for conserved DEUs between stages 10 and 15 is robust for finding

Development (2021) 148, dev191619. doi:10.1242/dev.191619

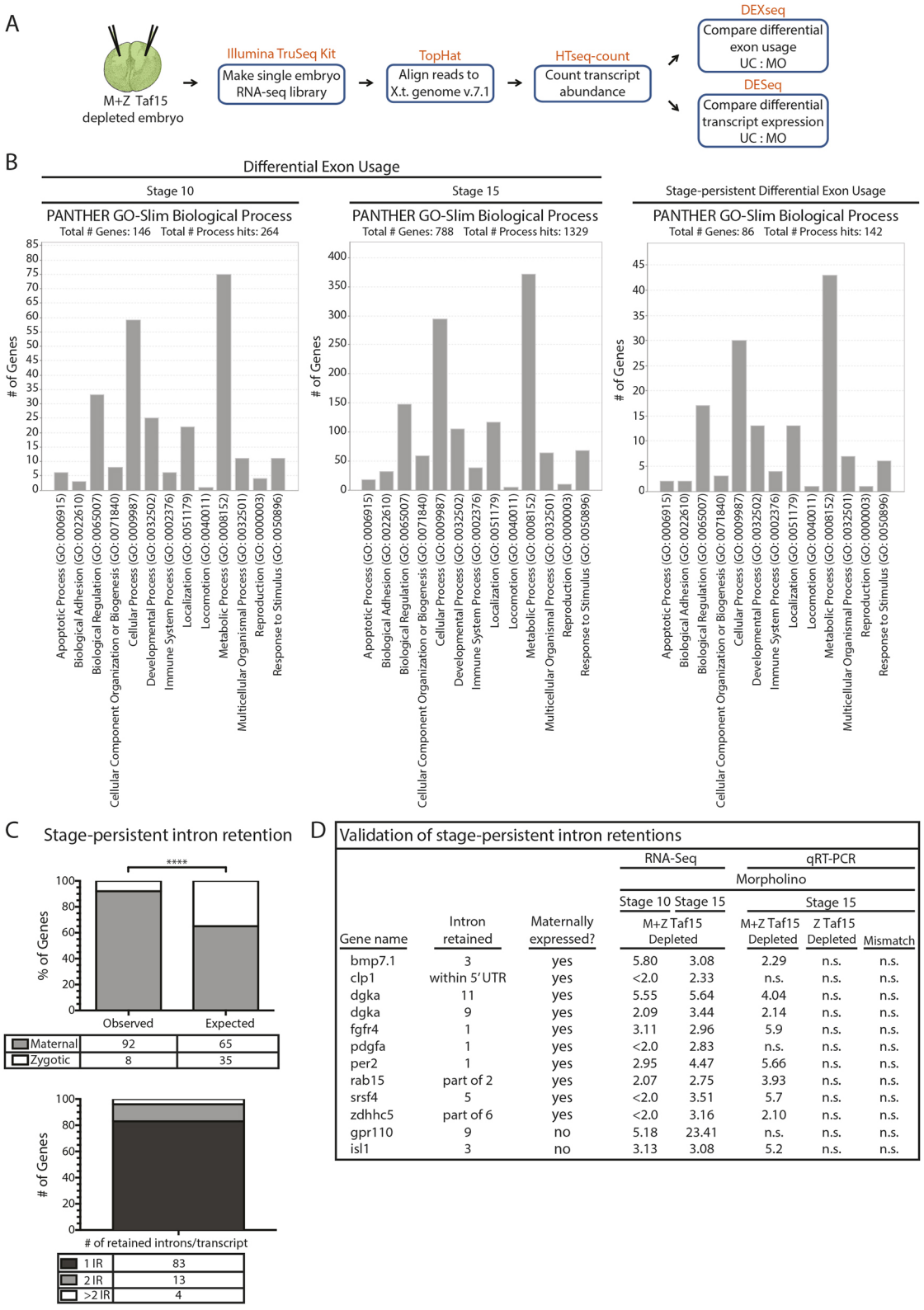

Gene name	Intron retained	Maternally expressed?	RNA-Seq Morpholino Stage 10 M+Z Taf15 Depleted	RNA-Seq Morpholino Stage 15 M+Z Taf15 Depleted	qRT-PCR Morpholino Stage 15 M+Z Taf15 Depleted	qRT-PCR Morpholino Stage 15 Z Taf15 Depleted	qRT-PCR Morpholino Stage 15 Mismatch
bmp7.1	3	yes	5.80	3.08	2.29	n.s.	n.s.
clp1	within 5′UTR	yes	<2.0	2.33	n.s.	n.s.	n.s.
dgka	11	yes	5.55	5.64	4.04	n.s.	n.s.
dgka	9	yes	2.09	3.44	2.14	n.s.	n.s.
fgfr4	1	yes	3.11	2.96	5.9	n.s.	n.s.
pdgfa	1	yes	<2.0	2.83	n.s.	n.s.	n.s.
per2	1	yes	2.95	4.47	5.66	n.s.	n.s.
rab15	part of 2	yes	2.07	2.75	3.93	n.s.	n.s.
srsf4	5	yes	<2.0	3.51	5.7	n.s.	n.s.
zdhhc5	part of 6	yes	<2.0	3.16	2.10	n.s.	n.s.
gpr110	9	no	5.18	23.41	n.s.	n.s.	n.s.
isl1	3	no	3.13	3.08	5.2	n.s.	n.s.

Fig. 2. Taf15 depletion by translation-blocking MO leads to intron retention. (A) Schematic of maternal (M) and zygotic (Z) Taf15 depletion via injection of translation-blocking MO and subsequent single-embryo RNA-seq analysis in *Xenopus tropicalis* embryos. (B) PANTHER GO-slim Biological Process classification of genes with differential exon usage following M+Z-Taf15 depletion. (C) Genes with intron retention in both stage-10 and -15 embryos classified by their M or Z expression, as well as the number of introns retained per transcript. ****P=1.50723E-08 (one-way ANOVA followed by Tukey post-hoc analyses). (D) qRT-PCR validation of RNA-seq results for genes with intron retention in both stage-10 and -15 embryos; qRT-PCR results expressed in fold change relative to uninjected controls; intron expression normalized to *eef1a1* and to respective total gene expression; n=3 individual embryos. All injections for downstream RNA sequencing and qRT-PCR analysis were into both cells of two-cell-stage embryos. IR, intron retention; n.s., not significant (one-way ANOVA followed by Tukey post-hoc analyses).

Development (2021) 148, dev191619. doi:10.1242/dev.191619

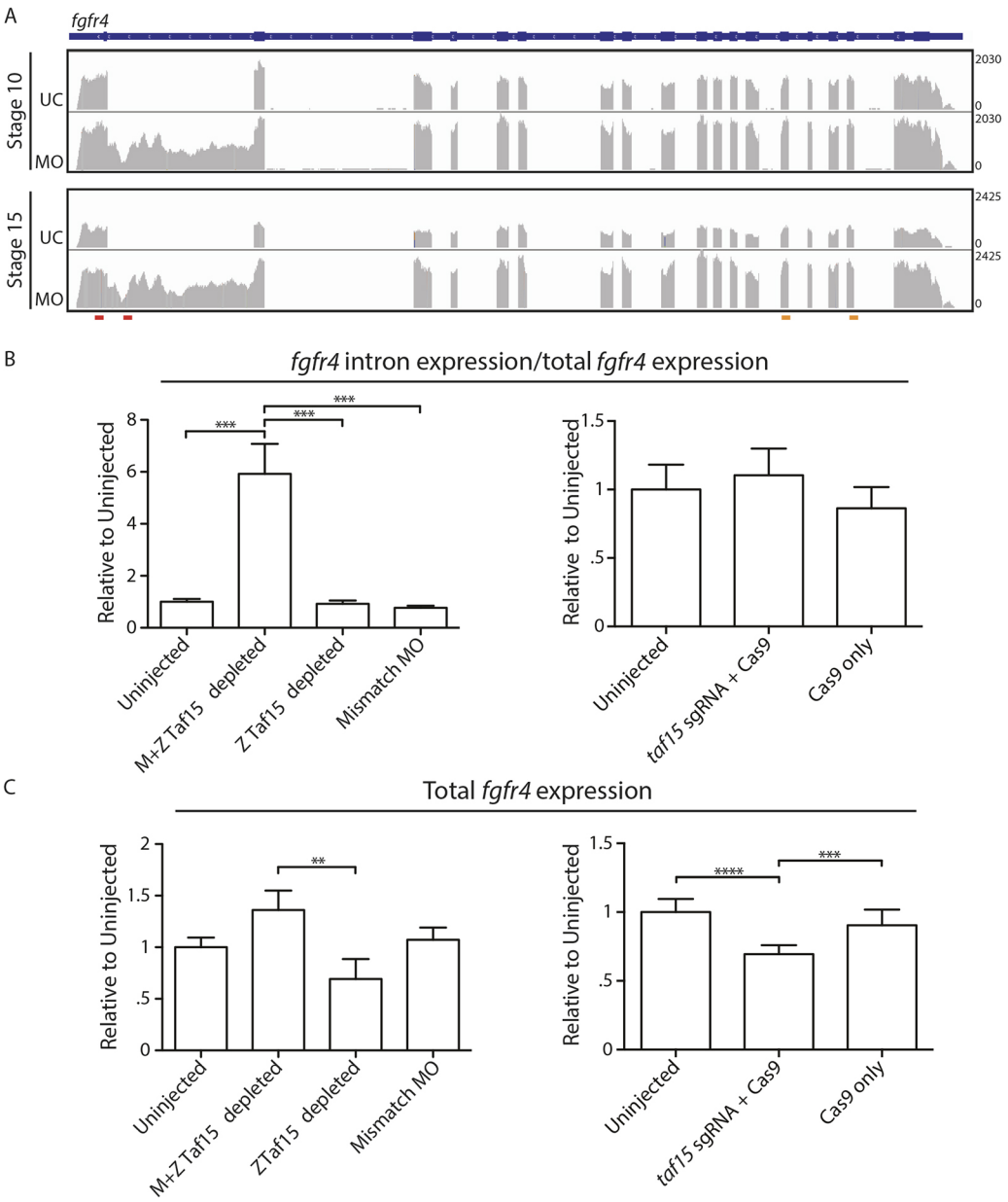

Fig. 3. Taf15 depletion by translation-blocking MO leads to single-intron retention in *fgfr4* in *Xenopus tropicalis* embryos. (A) Visualization of *fgfr4* RNA-seq reads with IGV aligned with the gene model in blue. Red bars indicate qRT-PCR primers used to measure retained introns. Orange bars indicate qRT-PCR primers used to measure total transcripts. (B) qRT-PCR for *fgfr4* intron 1 expression in stage-15 embryos. Intron expression levels are normalized to total *fgfr4* expression. ***P<0.0001. (C) qRT-PCR for total *fgfr4* expression in stage-15 embryos. **P<0.005, ***P<0.001, ****P<0.0001. In B,C, embryos treated as indicated on the *x*-axes; *y*-axes show *fgfr4* expression relative to *eef1a1* and normalized to uninjected embryos. Data are mean±s.d.; n=9 individual embryos. All means were compared by one-way ANOVA followed by Tukey post-hoc analyses. All injections for downstream qRT-PCR analysis were into both cells of two-cell-stage embryos. MO, M+Z-Taf15-depleting MO; UC, uninjected control.

splicing events with an early and lasting effect throughout development. To ensure that we further investigated genes with true DEUs, we used quantitative (q)RT-PCR to validate a subset of the DEU candidates that were found by RNA-seq of Taf15-depleted embryos to have robustly retained introns (of which there were 29/100; Table S3, column 'Retained introns as visualized by DEXseq gene modeling'). Of these DEXseq RNA-seq results, 9/12 (75%) were validated by qRT-PCR (Fig. 2D). These 12 cases of intron retention corresponded to a total of 11 genes as a result of the validation of two introns belonging to *dgka*. Surprisingly, these qRT-PCR data led to the finding that intron retention was exclusively found in embryos following M+Z-Taf15 depletion; intron retention was never observed by qRT-PCR in embryos depleted of Z-Taf15 or injected with mismatch MO (Fig. 2D). In addition, we showed that the splice-blocking MO was specific to Z-Taf15 depletion only and did not have an effect on maternally deposited Taf15 (Fig. S1), further supporting our hypothesis that splice changes are due to dose dependence of Taf15, which requires translation of maternal *taf15* mRNA.

Depletion of M+Z-Taf15 leads to intron retention in *fgfr4*

A twofold expression cutoff was applied to the DEXseq and DEseq results (except for stage-10 DESeq) and the candidate genes were sorted by their adjusted P (padj) values. The DEXseq results

Development (2021) 148, dev191619. doi:10.1242/dev.191619

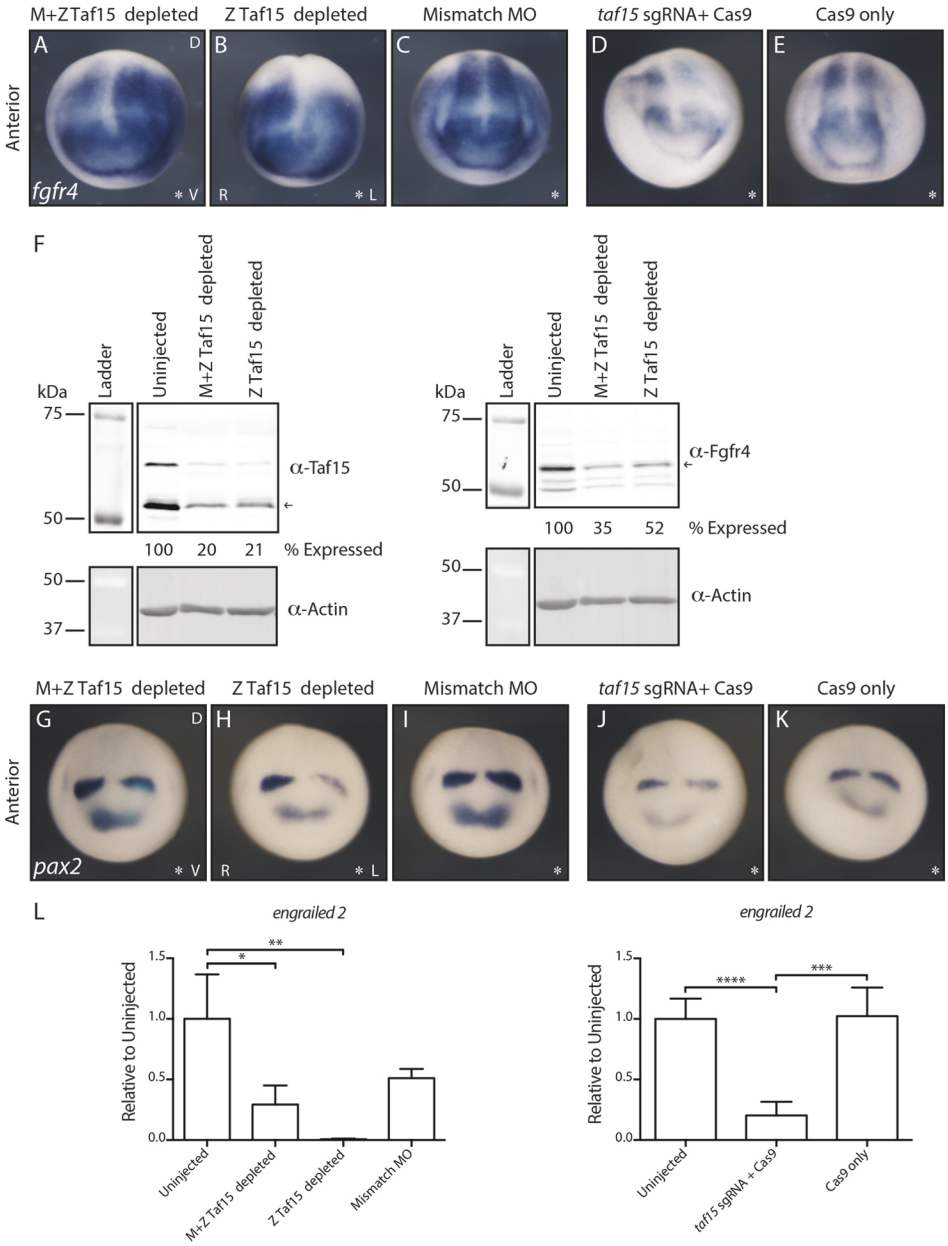

Fig. 4. Taf15 depletion leads to downregulation of *fgfr4* and its downstream targets. (A-E) Representative whole-mount ISH of *fgfr4* transcripts in Taf15-depleted *X. tropicalis* embryos; asterisks indicate the injected side. (F) Representative western blot for Taf15 and Fgfr4 expression in stage-15 Taf15-depleted embryos. Protein quantification is of the imaged blot using the most consistently expressed Taf15 or Fgfr4 band marked by a black arrow, normalized to the corresponding Actin band; percentage expression is relative to the uninjected condition; more than three blots were analyzed. (G-K) Representative whole-mount ISH of *pax2* transcripts in Taf15-depleted *X. tropicalis* embryos. Asterisks indicate the injected side. (L) qRT-PCR for *en2* expression in stage-15 embryos treated as indicated on the *x*-axes; *y*-axes show expression relative to *eef1a1* and normalized to uninjected embryos; *n*=6 individual embryos. Data are mean±s.d.; **P*<0.05; ***P*<0.002; ****P*<0.001; *****P*<0.0001. All means were compared by one-way ANOVA followed by Tukey post-hoc analyses. (A-E,G-K) Representative images of more than 12 embryos. All injections for downstream RNA ISH were into one cell of two-cell-stage embryos; the uninjected cell served as an internal control. (F,L) All injections for downstream qRT-PCR analysis were into both cells of two-cell-stage embryos. D, dorsal; L, left; R, right; V, ventral.

indicated *fgfr4* intron 1 to be the first and seventh hit in stage-10 and -15 embryos, respectively (Tables S1, S2). Numerous top-ranking candidate DEUs were visualized using the Integrative Genomics Viewer (IGV) and DEXseq DEU models at both stage 10 and stage 15 to gauge the significance of each DEU. Of these top candidates, *fgfr4* displayed the most robust intron retention (Figs S2, S3). In addition, *fgfr4* was an intriguing candidate because it is known that FGFRs are alternatively spliced. Examining the levels of *fgfr4* expression, DESeq results indicated the *fgfr4* transcript to be the 133rd and 20th hit in stage-10 and -15 embryos, respectively (Tables S4, S5). These results were validated by qRT-PCR in single M+Z-Taf15-depleted embryos using *fgfr4* intron 1-specific primers; *fgfr4* intron 1 was assayed across all depletion conditions, but was not detected outside of the M+Z-Taf15-depletion condition (Fig. 3B). To confirm that the *fgfr4* intron 1 qRT-PCR results were specific to retention (as suggested by visualization by IGV; Fig. 3A) and not simply increased as a result of an overall upregulation of *fgfr4* pre-mRNA, the *fgfr4* intron 1 expression levels (*fgfr4* intron 1-specific primers, red primer set; Fig. 3A) were normalized to the total *fgfr4* expression levels (Fig. 3B; *fgfr4* total transcript-specific primers, blue primer set; Fig. 3A). As a result of normalizing *fgfr4* intron 1 expression to total *fgfr4* expression, conditions that did not retain the *fgfr4* intron 1 had a relative expression equal to 1 within this analysis (Fig. 3B). Consistent with our qRT-PCR findings in Fig. 2D, intron retention was not observed following Z-Taf15 depletion by either MO or sgRNA/Cas9 (Fig. 3B). Interestingly, however, loss of Z-Taf15 (by either MO or CRISPR/Cas9) led to an overall reduction in total *fgfr4* expression (Fig. 3C); these results contrast sharply with the increased expression and intron retention of *fgfr4* following M+Z-*taf15* depletion (Fig. 3C). Importantly, *fgfr4* expression was unaffected following injection of control MO or Cas9 protein alone, suggesting that the changes in *fgfr4* expression are specific to Taf15 depletion (Fig. 3B,C).

We next used RNA ISH of total *fgfr4* to determine how the changes observed by qRT-PCR and RNA-seq following Taf15

Development (2021) 148, dev191619. doi:10.1242/dev.191619

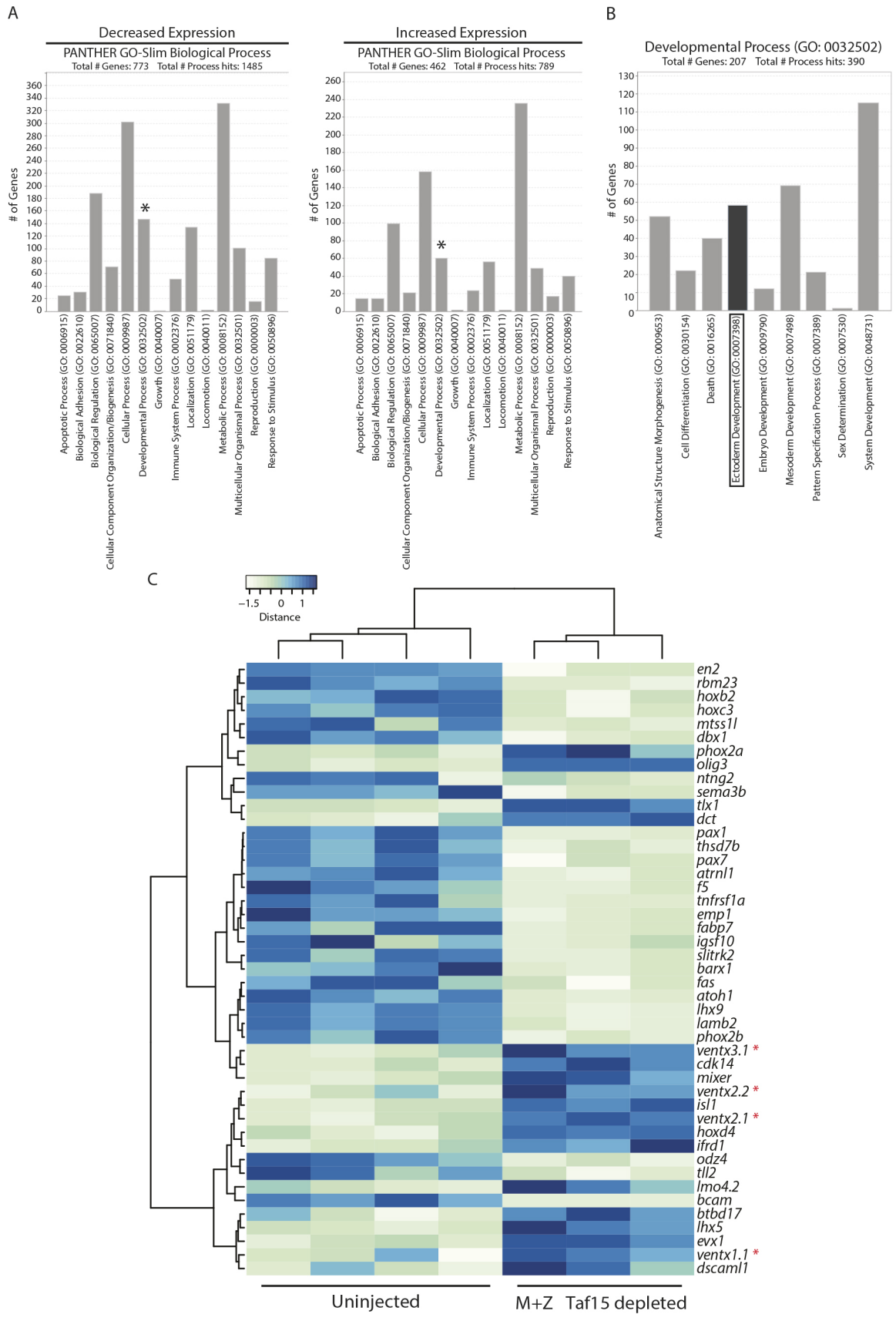

Fig. 5. Taf15 depletion leads to upregulation of the Ventx family of transcription factors. (A) PANTHER GO-slim Biological Process classification of differentially expressed genes in stage-15 *Xenopus tropicalis* embryos following M+Z-Taf15 depletion. Asterisks mark Developmental Process genes detailed in B. (B) Developmental Process subcategories. Boxed Ectoderm Development genes are visualized in C. (C) Expression-level heatmap of Taf15 target genes involved in Ectoderm Development. Asterisks mark Ventx family members. Columns represent RNA-seq data from a single embryo.

Development (2021) 148, dev191619. doi:10.1242/dev.191619

depletion may affect the expression pattern of *fgfr4*. M+Z depletion of Taf15 led to an increase and expansion of the lateral domain of *fgfr4* expression immediately outside the neural plate (Fig. 4A). We hypothesize that the intron-containing *fgfr4* transcripts fail to undergo degradation (necessitating normalization of intron levels to total transcript to avoid artificially inflating the amount of retained intron measured by qRT-PCR in Fig. 3B) and are largely responsible for this diffuse increase in expression and also that these transcripts are nonfunctional forms of *fgfr4*; indeed, M+Z-Taf15 depletion resulted in reduced Fgfr4 protein levels as measured by western blot (Fig. 4F). Following zygotic depletion of Taf15 by MO or sgRNA/Cas9, we observed a decrease in *fgfr4* transcript and protein (assayed for morphants only) expression (Fig. 4B,D,F). Importantly, *fgfr4* expression was unaffected following injection of control MO or Cas9 protein alone, suggesting that these results are specific to Taf15 depletion (Fig. 4C,E). These results are also consistent with the qRT-PCR data and suggest that the *fgfr4* transcripts are universally affected in each Taf15-depleted embryo, because the pattern of expression is largely unaffected (lateral expansion of *fgfr4* adjacent to the neural plate was observed in Z-Taf15-depleted morphant embryos, suggesting a modest delay in convergence, given that we observed complete neural tube closure). These findings further showed that both M+Z and Z-Taf15 MO depletion led to a loss of Fgfr4 (Fig. 4F); we hypothesize that this reduction is achieved through two different mechanisms: M+Z-Taf15 depletion leads to intron retention in *fgfr4*, resulting in an early stop codon and in reduced Fgfr4, whereas Z-Taf15 depletion leads to a reduction of total *fgfr4* mRNA expression, also resulting in reduced Fgfr4.

Lastly, after determining that total Fgfr4 expression was reduced following both M+Z- and Z-Taf15 MO depletion, we investigated whether downstream targets of Fgfr4 were affected. Indeed, ISH and qRT-PCR showed a reduction of the two midbrain/hindbrain markers,

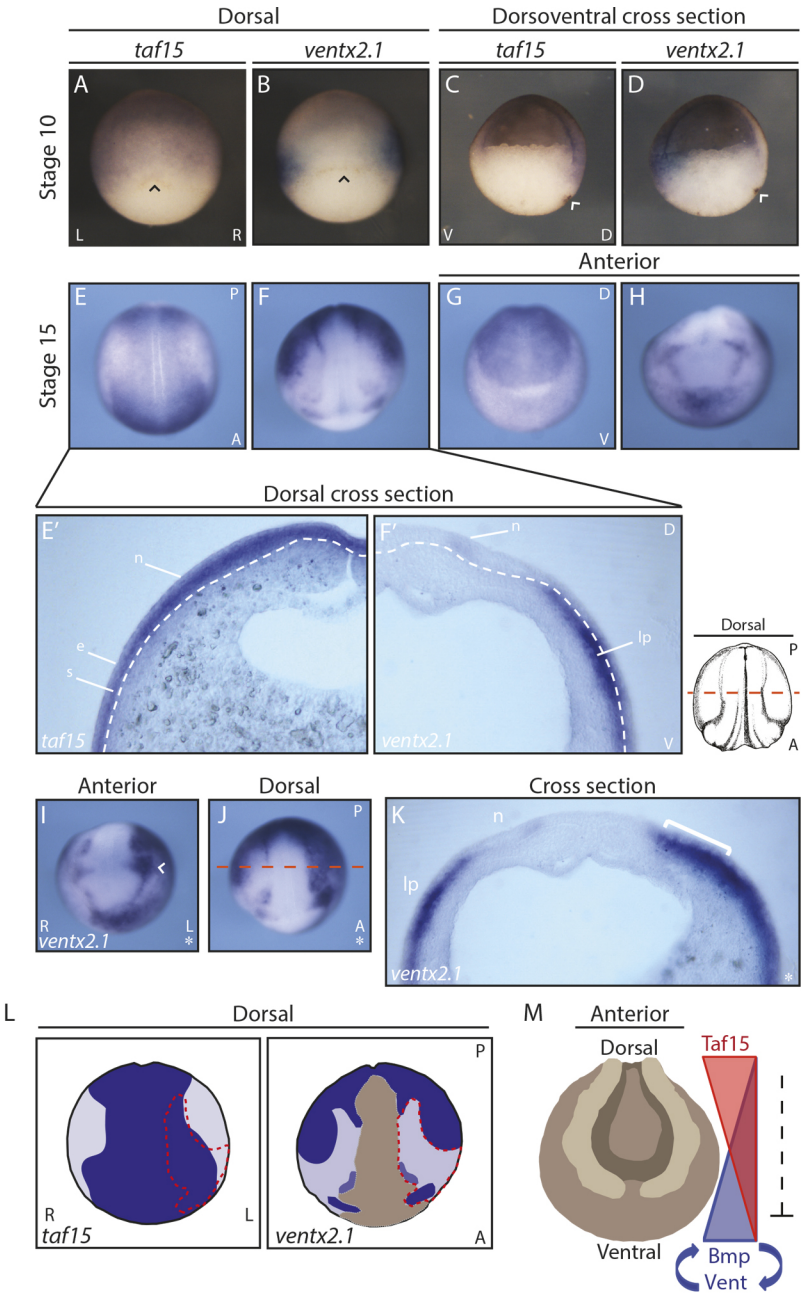

Fig. 6. *taf15* and *ventx2.1* exhibit complementary expression patterns and Taf15 depletion leads to expansion of *ventx2.1* expression into the neuroectoderm. (A,C,E,E′,G) Whole-mount ISH of *taf15*. (B,D,F,F′,H,I,J,K) Whole-mount ISH of *ventx2.1*. Black and white arrowheads in A, B, and C,D, respectively, indicate the dorsal lip. Dashed-white lines indicate the boundaries between the neural ectoderm and lateral plate mesoderm; dashed orange line indicates the site of the cross-sections. Asterisks indicate the injected side. White arrowhead in I indicates the eye anlage. White bracket in K indicates expanded *ventx2.1* expression. (L) Schematic comparing *taf15* and *ventx2.1* expression. Dark blue indicates stronger expression and light purple indicates weaker expression; dashed-red line indicates the region of *ventx2.1* expansion; brown indicates background level expression. (M) Model of Taf15 repression in the ventrolateral Bmp/Vent circuit. Representative images of more than 12 embryos in A-H,I,J, and more than five cross-sectioned embryos in E′,F′,K. All injections for downstream RNA ISH were into one cell of two-cell-stage embryos in I,J,K; the uninjected cell served as an internal control. A, anterior; D, dorsal; e, epithelial layer of the epidermal ectoderm; L, left; lp, lateral plate mesoderm; n, neural ectoderm; P, posterior; R, right; s, sensorial layer of the epidermal ectoderm; V, ventral.

Development (2021) 148, dev191619. doi:10.1242/dev.191619

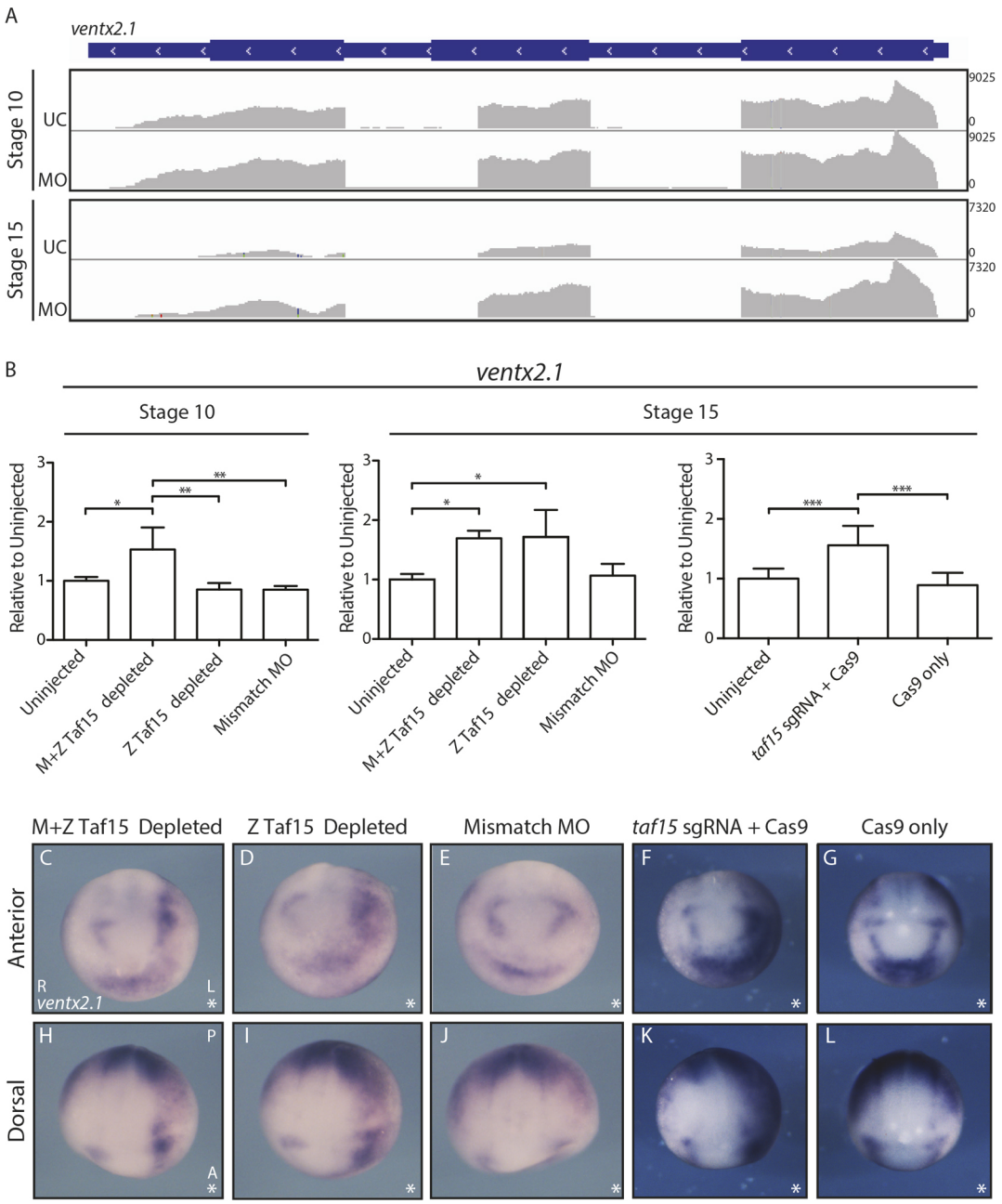

Fig. 7. Taf15 depletion leads to increased and expanded *ventx2.1* expression. (A) Visualization of *ventx2.1* RNA-seq reads with IGV aligned with the gene model in blue. (B) qRT-PCR for *ventx2.1* expression in stage-10 and -15 embryos treated as indicated on the *x*-axes; *y*-axes show expression relative to *eef1a1* and normalized to uninjected embryos; *n*=9 individual embryos; Data are mean±s.d; **P*<0.05; ***P*<0.005; ****P*<0.001. All means were compared by one-way ANOVA followed by Tukey post-hoc analyses. All injections were into both cells of two-cell-stage embryos. (C-L) Representative whole-mount ISH of *ventx2.1*; asterisks indicate the injected sides. Images are representative of more than 12 embryos. All injections for downstream RNA ISH were into one cell of two-cell-stage embryos; the uninjected cell served as an internal control. A, anterior; L, left; MO, M+Z Taf15-depleting MO; P, posterior; R, right; UC, uninjected control.

pax2 and *en2*, across all Taf15-depletion conditions (Fig. 4G-L) (Hongo et al., 1999). These results indicate that M+Z- and Z-Taf15 depletion both lead to the downregulation of Fgfr4, but through independent mechanisms of transcriptional regulation.

We previously showed that 83% of stage-persistent DEUs were characterized by the retention of a single intron (Fig. 2C); this was consistent with what was observed in *fgfr4*. A broader analysis determined whether first introns are preferred targets or whether *fgfr4* is an exception. In examining the top-ten genes with affected DEUs (as sorted by padj-value) at both embryo stages 10 and 15, we found that the single retained introns were not restricted to first introns, but were dispersed in different transcripts (Figs S2, S3; Table S7). Therefore, retention of a single intron was the most common characteristic of DEU following M+Z-Taf15 depletion (13/20 cases) within this cohort, contrasting with the effects of Fus depletion, which affects all introns of DEU genes.

Measuring changes in gene expression following Taf15 depletion

It is unknown whether and how the FET family of proteins regulates levels of gene expression in *Xenopus*. Our data thus far suggest that Taf15 controls both mRNA splicing and overall levels of a

Development (2021) 148, dev191619. doi:10.1242/dev.191619

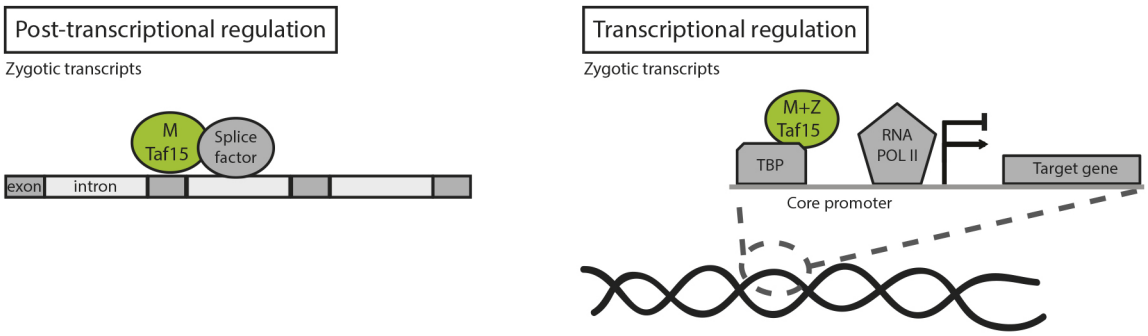

Fig. 8. Model of Taf15 pre- and post-transcriptional regulation where Taf15 binds to the pre-mRNA or the core promoter, respectively. M Taf15, maternal Taf15; M+Z Taf15, maternal and zygotic Taf15; TBP, TATA-binding protein.

subset of RNAs in the developing embryo. Concurrent with analyzing how Taf15 depletion affects changes in intron/exon usage (DEXseq), we also examined levels of transcript abundance using DESeq (Fig. 5).

Following DESeq analysis, to focus on a few candidate genes that exhibited differential expression following Taf15 depletion, a twofold threshold cutoff was applied to the differentially expressed gene candidates, followed by PANTHER GO-slim Biological Process analysis. In stage-15 embryos, 2094 transcripts were found to exhibit a twofold increase or decrease in gene expression (Table S6), 1235 of which were assigned a PANTHER GO-slim Biological Process (Fig. 5A; a total of 773 genes with decreased expression plus 462 genes with increased expression). Our *taf15* ISH data suggested that *taf15* has a specific expression pattern; therefore, we looked more closely at those genes that fell under the PANTHER GO-slim Developmental Process (Fig. 5A, asterisk); 207 genes were found to be differentially expressed within this classification (Fig. 5B; combined developmental process results from Fig. 5A). More specifically, our *taf15* ISH data suggested that *taf15* is expressed in the ectoderm at stage 15 (Fig. 1A, stage 15); therefore, the subset of transcripts annotated with the ectoderm development classification were examined more closely (Fig. 5B,C). One family of genes in this category, which increased in expression following M+Z-Taf15 depletion, was the VENT family of homeodomain transcription factors (Ventx genes), suggesting a role for Taf15 suppression of Ventx gene expression in the ectoderm (Fig. 5C). Interestingly, Ventx genes act in a positive-feedback loop with the bone morphogenetic proteins (Bmps), which specify the ventral domain of the *Xenopus* embryo (Onichtchouk et al., 1998; Sander et al., 2007). Given that *taf15* is expressed in the future dorsal domain of the gastrula (Fig. 1A), we were intrigued to find a gene family (Ventx) that functions in ventral tissue development and is upregulated upon Taf15 depletion. This suggests an early and lasting regulatory relationship between *taf15* and Ventx genes. Of the four Ventx gene paralogs upregulated following M+Z-Taf15 depletion, *ventx2.1* acts upstream of *ventx1.1*, *ventx2.2* and *ventx3.1*; therefore, we investigated the relationship between *ventx2.1* and *taf15* further (Schuler-Metz et al., 2000).

Taf15 regulates dorsoanterior development by repressing *ventx2.1*

To better understand the relationship between *taf15* and the Ventx genes, we analyzed their expression patterns further. ISH revealed a subset of complementary expression patterns between *taf15* and *ventx2.1*, consistent with inhibition of *ventx2.1* by Taf15 (Fig. 6A-H). In stage-10 embryos, *taf15* was expressed in the embryonic domain that gives rise to future dorsal structures, whereas *ventx2.1* expression was markedly absent from this region and instead was found in the embryonic domain that gives rise to future ventral structures (Fig. 6A-D). The complementary expression of *ventx2.1* and *taf15* continued into the neurula stage (Fig. 6E-H). To visualize the extent of complementary expression, medial cross-sections along the dorsoventral axis of stage-15 embryos were made following ISH. These sections revealed that *taf15* was strongly expressed throughout the neuroectoderm and in both the epithelial and sensorial layers of the ectoderm, whereas *ventx2.1* was strongly expressed in the underlying lateral plate mesoderm and only faintly expressed in a portion of the neuroectoderm (Fig. 6E′,F′). One domain in which *taf15* and *ventx2.1* exhibited overlapping expression was in the forebrain (Fig. 6E-H).

Having established by RNA-seq that *ventx2.1* expression increased with M+Z-Taf15 depletion and that *taf15* and *ventx2.1* have some complementary expression patterns, we examined *ventx2.1* expression *in situ* in Taf15-depleted embryos. Embryos with depleted M+Z-Taf15 showed increased *ventx2.1* expression in regions that normally have strong *taf15* and weak *ventx2.1* expression, specifically below the lateral neuroectoderm and prospective epidermal region [Fig. 6E,F,J,K (white bracket) and L]. In addition, *ventx2.1* expression increased in the region of the forebrain in which *taf15* and *ventx2.1* are co-expressed [Fig. 6G,H,I (arrowhead) and L]. Taken together, these data suggest that Taf15 suppresses *ventx2.1* and does so indirectly, given that the genes are expressed in adjacent germ layers. The increased level of *ventx2.1* was consistent with the gross phenotype of reduced head structures observed in older Taf15-depleted embryos (Fig 1D,E, Fig 6L, red outline).

Taf15 regulates *ventx2.1* throughout early embryogenesis

RNA-seq data showed that M+Z-Taf15 depletion resulted in increased *ventx2.1* expression by neurula stage 15 but not during the earlier gastrula stage 10 (less than a twofold change) (Fig. 7A). However, qRT-PCR results showed that *ventx2.1* expression significantly increased at both stage 10 and 15 following M+Z-Taf15 depletion (Fig. 7B), consistent with the complementary *taf15* and *ventx2.1* expression patterns observed by ISH at stage 10 (Fig. 6A-D). Following Z-Taf15 depletion, *ventx2.1* expression was unaffected at stage 10 (based on qRT-PCR); however, by stage 15, Z-Taf15-depleted embryos phenocopied those that were M+Z-Taf15 depleted (Fig. 7B). We hypothesize that the effects of Z-Taf15 depletion on embryonic development were not observed as early as stage 10 because zygotic genome transcription had only just begun (possibly not giving the zygotic genome-targeting MO enough time to act); furthermore, maternal Taf15 could still be present and able to suppress the transcription of *ventx2.1*. Embryos injected with a mismatch MO to the translation start site of *taf15* did

Development (2021) 148, dev191619. doi:10.1242/dev.191619

not exhibit changes in *ventx2.1* expression at either stage, suggesting that the changes in gene expression observed in M+Z- and Z-Taf15-depleted embryos are specific to MO-mediated Taf15 depletion (Fig. 7B,E,J).

To ensure that the increase in *ventx2.1* expression was not a MO-specific effect, we measured *ventx2.1* expression following Taf15 depletion with CRISPR/Cas9. qRT-PCR data for *ventx2.1* expression in stage-15 sgRNA+Cas9-injected embryos was similar to those observed in M+Z- and Z-Taf15-depleted embryos; importantly, injection of Cas9 alone did not affect the *ventx2.1* expression level (Fig. 7B). In addition to quantifying the changes in *ventx2.1* expression by qRT-PCR, the embryonic expression pattern of *ventx2.1* was also compared between MO and CRISPR/Cas9 conditions. We found that the expression pattern of *ventx2.1* following sgRNA *taf15+Cas9* phenocopied that of M+Z- and Z-Taf15-depleted embryos (Fig. 7C-L). Taken together, these qRT-PCR and ISH data suggest that changes in *ventx2.1* expression are specific to Taf15 depletion and that both M- and Z-Taf15 play a role in suppressing the expression of *ventx2.1* throughout development.

DISCUSSION

Previous to our investigation, few studies had focused on the role of TAF15 in development. TAF15 is not considered a canonical TAF because it is not associated with all human TFIID complexes and has no ortholog in invertebrate species (Ballarino et al., 2013). However, it is this nonubiquitous association with the core transcriptional machinery that interests us because this supports the hypothesis that TAF15 may be selective in the transcripts it regulates and, as a result, may have specific roles in development. TAF15 would not be the first TAF to be shown to have a specific role in development; for example, TAF3 is required for endoderm lineage differentiation and for preventing the premature specification of neuroectoderm and mesoderm in embryonic stem cells (Liu et al., 2011).

The analysis presented here demonstrates that Taf15 is deposited maternally in *Xenopus* eggs and is later expressed zygotically. We further show that Taf15 has an enriched expression pattern within the developing embryo, with maternal *taf15* preferentially expressed in the animal hemisphere and zygotic *taf15* enriched dorsally during gastrulation, throughout the neural ectoderm during neurulation and in dorsoanterior tissues during the tailbud and tadpole stages. Consistent with the expression pattern of *taf15*, we found that embryos depleted of *taf15* have defects in head structures, such as reduced fore/midbrain and eyes by the early tadpole stage. Interestingly, by using RNA-seq to understand the role of Taf15 in development, we made the surprising discovery that M- and Z-Taf15 use different mechanisms to regulate Fgfr4 expression: the co-depletion of M- and Z-Taf15 downregulates Fgfr4 expression at the post-transcriptional level via the retention of a single *fgfr4* intron, whereas depletion of Z-Taf15 alone downregulates Fgfr4 expression through the reduction of the total *fgfr4* transcript. In addition, we found that Taf15 is required to repress *ventx2.1* from dorsal and neural ectodermal tissues and that *taf15* and *ventx2.1* exhibit a complementary expression pattern throughout gastrulation and neurulation. The data presented here suggest that Taf15 plays an integral and pleiotropic role in development of the dorsoanterior neural tissues and further suggest that the mechanism of gene regulation by Taf15 is target dependent and subject to the milieu of factors that are present at different stages of development, likely as a result of the presence of specific co-factors required for activity (Fig. 8).

It is not unexpected that Taf15 plays a pleiotropic role in *Xenopus* development because FET proteins are associated with regulating numerous cellular activities, including cell proliferation, cell cycling, cell death, transcription, splicing, microRNA processing, RNA transport, signaling and maintenance of genomic integrity (Andersson et al., 2008; Ballarino et al., 2013; Gregory et al., 2004; Shiohama et al., 2007). Furthermore, we expected that splicing could be a shared mechanism of gene regulation between Fus and Taf15 in *Xenopus* development because studies using photoactivatable ribonucleoside-enhanced cross-linking and immunoprecipitation (PAR-CLIP) found that FET proteins predominantly bind to intronic regions as well as the 3′-untranslated region (UTR) of genes (Hoell et al., 2011). However, we were surprised by how differently the two FET family members, Fus and Taf15, affect *Xenopus* development: embryos depleted of Fus fail to undergo gastrulation because of the retention of all introns in a subset of target genes required for mesoderm differentiation and epithelial adhesion (Dichmann and Harland, 2012), whereas embryos depleted of Taf15 survive into the tadpole stage and exhibit defects specific to dorsoanterior head development resulting, in part, from dysregulation of *fgfr4* and *ventx2.1*; and, in contrast to Fus, Taf15 depletion affects a subset of specific introns.

Taf15 provides an example of a gene product with two different mechanisms (post-transcriptional or transcriptional) by which it regulates the expression of the same target gene (*fgfr4*). Furthermore, we show that the mode of regulation is dependent on whether Taf15 is maternally deposited or zygotically transcribed. Although there are classic examples of genes having separable maternal and zygotic developmental roles (e.g. *CTNNB1*) (Heasman et al., 1994, 2000), we are unaware of a case in which the mechanism of regulatory action changes while the target remains the same.

Classical RNA splicing can be separated into two functional types: constitutive and alternative splicing. Constitutive splicing is the process by which introns are removed (spliced), stitching together exons in the same order that they are found in the genome and producing one gene product (Boutz et al., 2015; Pandya-Jones, 2011; Perales and Bentley, 2009). Alternative splicing refers to the process by which exons of a gene may be included or excluded, producing numerous gene products (isoforms) and increasing gene product diversity and complexity (Black, 2003; Grabowski and Black, 2001). Both constitutive and alternative splicing occur co-transcriptionally, prior to the transcriptional termination and polyadenylation of pre-mRNAs (Pandya-Jones and Black, 2009). In addition to co-transcriptional splicing, there is also post-transcriptional splicing. It has been shown that the retention of individual introns in polyadenylated pre-mRNAs serves as a mechanism for controlling gene expression: transcripts with retained introns remain in the nucleus, preventing translation of the transcript; following a cellular signal (e.g. osmotic or heat stress), the intron is excised and the protein is quickly translated (Boutz et al., 2015; Ninomiya et al., 2011). Here, we closely studied *fgfr4*, a transcript that is both maternally deposited and zygotic transcribed, and observed post-transcriptional splicing defects (in *fgfr4* as well as other targets) following the depletion of M+Z-Taf15. Our RNA-seq data, generated from post-ZGA embryos (stages 10 and 15), support a model in which translation of maternally deposited *taf15* is required for the proper post-transcriptional splicing of nascent zygotic pre-mRNA transcripts during ZGA. Indeed, in looking at early RNA-seq datasets (Xenbase; http://www.xenbase.org/), we find no evidence that any of the maternal transcript (e.g. *fgfr4*) is incompletely spliced.

In the embryonic environment, in which ZGA occurs and, therefore, active transcription is taking place, we propose that both

Development (2021) 148, dev191619. doi:10.1242/dev.191619

maternally deposited Taf15 and Taf15 translated post-fertilization aid in splicing the new (zygotic) transcripts (e.g. *fgfr4*, *isl1* and others; Figs S2, S4), resulting in unspliced transcripts at stage 10 after Taf15 depletion, but that zygotic Taf15 acts more classically and likely associates with the core promoter, using either its N-terminal low-complexity domain or RNA-binding domains to bind the C-terminal domain of RNA Pol II, regulating transcription of specific targets (Fig. 8). Upon ZGA (i.e. production of nascent transcripts), zygotic Taf15 may associate with the core promoter to regulate the expression of zygotically transcribed targets (e.g. *fgfr4*) (Fig. 8). Our data also show that there is not always a discrepancy in M-Z-Taf15 target regulation. In the case of *ventx2.1*, which is expressed zygotically (and not maternally deposited), we did not observe a splicing defect following Taf15 depletion and found that M+Z-Taf15 depletion results in increased *ventx2.1* expression.

We now know that at least one member of the FET family of atypical RNA-binding proteins, Taf15, is required to regulate dorsoventral patterning in *Xenopus*. *Xenopus* embryos depleted of Taf15 have a phenotype similar to that observed when embryos are depleted of the Bmp antagonist Chordin or of pairs of Bmp antagonists (Reversade et al., 2005; Khokha et al., 2005). Both Chordin and Taf15 depletion result in ventralized embryos with reduced head and eye structures as well as reduced dorsal and posterior fin and tail structures. As with Taf15 depletion, Chordin-depleted embryos have a relatively normal cement gland and increased ventral tissue. Interestingly, according to our RNA-seq data, Taf15-depleted embryos do not decrease Chordin expression; in fact, we observed a twofold increase in stage-15 embryos (Tables S4, S6). However, rather than regulating Bmps directly, we suggest a model in which Taf15 is needed to repress Ventx genes, thereby disrupting the Bmp/Vent positive-feedback loop (Fig. 6M) (Schuler-Metz et al., 2000). These data clearly illustrate the role of Taf15 in regulating dorsoventral patterning. We also propose a model in which Taf15 represses *ventx2.1* from the dorsal marginal zone of the gastrula, repression that continues throughout neurulation, given that Taf15 represses *ventx2.1* from dorsal neural ectodermal tissue. Without knowing whether Ventx genes are direct transcriptional targets of Taf15, we cannot conclude whether the function of Taf15 is to repress, or activate a repressor of, Ventx gene expression. However, the RNA-seq results show that there is no intron retention in the Ventx genes, which supports the conclusion that the RNA-splicing activity of Taf15 does not control the Taf15-dependent repression of *ventx2.1*.

Interestingly, the human Vent-like homeobox gene *VENTX*, a putative homolog of *Xenopus ventx2*, is aberrantly expressed in CD34+ cells of patients with acute myeloid leukemia (Rawat et al., 2010). Furthermore, the leukemia-associated TAF15 fusion protein, TAF15-CIZ/NMP4, is also found in acute myeloid leukemia (Alves et al., 2009). Although the Ventx gene has been lost in mouse, its function in repressing dorsal fates is well conserved between fish and frogs (Imai et al., 2001; Rawat et al., 2010). Given the relationship observed between increased Ventx gene expression following Taf15 depletion, the coincidence of TAF15 dysfunction and increased *VENTX* in acute myeloid leukemia and that Ventx is required for proper mesenchyme and blood differentiation in *Xenopus*, it is possible that Taf15-dependent negative regulation of Ventx genes is a conserved mechanism (Onichtchouk et al., 1998).

In summary, the data presented here show that a target gene (*fgfr4*) is regulated through two different molecular mechanisms (post-transcriptionally or transcriptionally) depending on the mechanism of Taf15 depletion (M+Z or Z). We have also demonstrated that, although the effects of Taf15 on development are pleiotropic, consistent with our observations that embryos exhibit reduced head structures following Taf15 depletion, we identified two specific pathways by which Taf15 regulates dorsoanterior brain development (*fgfr4* and *ventx2.1*). Furthermore, we have demonstrated that the FET family of atypical RNA-binding proteins do not act redundantly in regulating *Xenopus* development; Taf15- and Fus-depleted embryos exhibit very distinct phenotypes as well as mechanisms of gene expression regulation. Our findings of nonoverlapping transcriptional effects of Taf15 and Fus in *Xenopus* support the idea that the disease consequences resulting from chromosomal translocations involving the FET family of proteins are unlikely to be common transcriptional effects, but are more likely to result from the similar cellular aggregates of mutant proteins (Scekic-Zahirovic et al., 2016; Sharma et al., 2016; Svetoni et al., 2016).

MATERIALS AND METHODS

Ethics statement

This study was carried out in strict accordance with the recommendations in the Guide for the Care and Use of Laboratory Animals of the National Institutes of Health. The protocol was approved by the Animal Care and Use Committee at the University of California, Berkeley.

General *Xenopus* embryo culture

Xenopus tropicalis embryos were obtained through natural matings. For next-day (daytime) matings, males were housed individually and females were housed together in 4 l Rubbermaid containers filled with 2 l of water collected from the *X. tropicalis* housing racks. The night before the natural mating, males were boosted with 100 U of human chorionic gonadotropin (HCG: Chorulon, Merck & Co., NADA 140-927, 133754) and females were primed with 10 U HCG. The morning of mating, females were boosted with 200 U HCG and paired with males. *X. tropicalis* embryos were collected using a disposable polyethylene transfer pipet (Fisherbrand; Fisher Scientific, 13-711-7 M), with the tip cut off to enlarge the opening. Embryos were dejellied and cultured as previously described (Khokha et al., 2002) until the desired stage according to the normal table of development (Nieuwkoop and Faber, 1994).

Whole-mount RNA *in situ* hybridization

Embryos were fixed in MEMFA (0.1 M MOPS pH 7.4, 2 mM EGTA, 1 mM $MgSO_4$, 3.7% v/v formaldehyde) as previously described (Sive et al., 2000). RNA probes were labeled with digoxigenin-UTP (Roche, 11277073910) and chromogenic reactions were carried out by incubating hybridized embryos in anti-digoxigenin-AP Fab fragments, 1:3000 (Roche, 11 093 274 910) and the alkaline phosphatase substrate BM Purple (Roche, 11 442 074 001), as previously described (Sive et al., 2000). Embryos were prehybridized for at least 1 h.

Western blotting

Embryos were lysed in 20 mM Tris-HCl (pH 8.0), 50 mM NaCl, 2 mM EDTA, with 1× protease inhibitor (Roche cOmplete, Mini, EDTA-free, 11836170001), with 20 µl per embryo 1% Triton X-100 detergent (freshly added; Sigma-Aldrich, T8787), homogenized by pipetting and freezing at −80°C. To pellet debris, lysates were spun at 2655 ***g*** (Eppendorf Centrifuge, 5417C) at 4°C and the supernatant was transferred to a new tube. To clear embryos of yolk, lysates were spun at 2655 ***g*** an additional two to three times, each time using a vacuum with a nonfiltered p200 tip to remove the yolk briskly from the top of the lysate. Lysate protein concentrations were measured with Bradford assays (Bio-Rad Protein Assay Dye Reagent Concentrate, 500-0006) and read using a Molecular Devices, SpectraMax M2 plate reader, as per manufacturer's instructions. Lysates were aliquoted for use and 6× loading dye was added. The samples were then heated at 80°C for 10 min. Lysates were run on an 8% polyacrylamide gel at 120 V for 105 min, eliminating proteins of 10-20 kDa. Proteins were transferred from gels using a semi-dry transfer

Development (2021) 148, dev191619. doi:10.1242/dev.191619

system (Bio-Rad Trans-Blot® SD Semi-Dry Electrophoretic Transfer Cell, 170-3940) to Immobilon®-FL transfer membranes, PVDF (Millipore, IPFL00010), and blocked for 1 h at room temperature with 1× Odyssey® Blocking Buffer (PBS) (LI-COR, 927- 40000). Membranes were incubated overnight at 4°C with anti-Taf15 (TAFII68) antibodies (1:3000; Bethyl Laboratories, A300-309A), anti-Fgfr4 (CD334) antibodies (1:2000; Thermo Fisher Scientific, PA5-28175) and anti-β-Actin antibodies (1:5000; GeneTex, clone GT5512, GTX629630), diluted in 5% bovine serum albumin (BSA) in TBS-tween (TBS-T; 0.1% Tween 20). Fluorescent secondary antibodies [Alexa Fluor® 680 goat anti-rabbit IgG (Invitrogen, A-21109), IRDye® 800CW donkey anti-mouse IgG (LI-COR, 925-32212)] were incubated at 1:10,000 for 1 h at room temperature in the dark. Western blots were visualized and quantified using a LI-COR Odyssey imager and software.

Microinjection of morpholino antisense oligonucleotides: maternal and/or zygotic Taf15 depletion

MOs were designed and ordered from GeneTools LLC. *taf15* translation-blocking (M and Z) MO: 5′-AGCTACTGGGATCTGAAGACATGAT-3′; *taf15* splice-blocking (Z only) MO: 5′-TTCCAAAACCTACCTTTG-TTGCTGC-3′; Mismatch MO: 5′-AGCTAGTCGCATCTCAACACAT-GAT-3′.

MOs were dissolved in nuclease-free water to 8.5 ng/nl (1 mM). Translation-blocking (17 ng/cell), splice-blocking (8 ng/cell) or mismatch (17 ng/cell) MOs were injected into either one or both cells of two-cell-stage embryos, to deplete target mRNA from half or the whole embryo, respectively. To trace which cells contained MO, each MO was co-injected with the fluorescein-conjugated standard control oligo (GeneTools).

RNA extraction

RNA from individual *X. tropicalis* embryos was isolated using the Trizol Reagent (Ambion, 15596026), optimized for extracting small amounts of RNA from single embryos. Single embryos were collected in 200 µl of Trizol Reagent, homogenized by pipetting and stored at −80°C for a minimum of 14 h. Homogenized samples were thawed and incubate at room temperature for 5 min to allow complete dissociation of the nucleoprotein complex. Then, 40 µl of chloroform was added to each sample, which was then vortexed and incubated at room temperature for 2-3 min. Samples were centrifuged at 12,000 ***g*** for 15 min at 4°C and 90 µl of the upper aqueous phase was removed and placed in a new tube. RNA was precipitated with 100% isopropanol with 5 µg of linear acrylamide (Ambion, AM9520) for pellet detection. RNA pellets were washed with 75% ethanol and air dried at room temperature for 5-10 min. RNA pellets were resuspended in 250 µl of Milli-Q water, gently pipetted up and down and then vortexed. A second RNA extraction was performed by adding 250 µl of acid-phenol: chloroform, pH 4.5 (with IAA, 125:24:1) (Ambion, AM9720) following the manufacturer's protocol. RNA was precipitated by adding 20 µl 5 M NH_4OAC (ammonium acetate) (Ambion, AM9070G) and 220 µl of 100% isopropanol and washed twice with 75% ethanol. RNA concentrations were measured using a nanodrop (Nanodrop ND-1000 Spectrophotometer) and used for RNA-seq library preparation or qRT-PCR.

RNA-seq library preparation and analysis

Each paired-end library for RNA-seq was prepared using RNA extracted from single *X. tropicalis* embryos; each sample comprised three to four independently sequenced embryos. RNA-seq libraries were made strictly following the Low Sample (LS) Protocol from the TruSeq RNA Sample Preparation v2 Guide. The important modification made to this protocol was that all reagents, except for the Bead Washing Buffer, were used at half volume.

Final RNA-seq libraries were quantified using the KAPA Library Quantification Kits for Illumina sequencing platforms (Roche, KK4824). Then, 100 bp paired-end sequencing reads (Illumina HiSeq2000) were aligned to the *X. tropicalis* genome version 7.1 (and an annotation from D.S.D., unpublished). RNA-seq data analysis for differential gene expression was performed using both the Tuxedo Suite (Tophat, Bowtie, Cufflinks, Cuffdiff; Illumina) (Trapnell et al., 2012) and the Bioconductor package DESeq (Love et al., 2014). RNA-seq data analysis for differential intron-exon usage was performed using the Bioconductor package, DEXseq (Reyes et al., 2014) (www.bioconductor.org). In brief, read counts were normalized to library size per feature. The *P*-values are the result of the statistical modeling performed by DESeq2/DEXSeq and indicate the degree to which the difference in expression of a given gene or exon was significant (in morphants compared with controls). The *P*-values were then adjusted for false discovery rates (also performed by DESeq2/DEXSeq) for the number of features, because false positive calls are problematic when sampling a large number of features (genes or exons), as is performed in gene expression studies.

RNA-seq alignments were visualized using the IGV from the Broad Institute (www.broadinstitute.org/igv/).

Complementary DNA (cDNA) synthesis and qRT-PCR

RNA was isolated from single embryos as described above. cDNA was synthesized using the iScript Reverse Transcription (RT) reaction protocol (Bio-Rad, 170-8841). Optimally, 1 µg of total RNA was reverse transcribed, but total RNA yield from a single *X. tropicalis* embryo varied. Therefore, all samples were normalized to ensure all RT samples contained the same volume and concentration of RNA. For each RT reaction, 7.5 µl of 5× iScript RT Supermix was added to 30 µl of RNA/H_2O. For no RT (NRT) samples, RNA samples with yields below a usable limit were pooled and the sample volume was brought up to 30 µl and 7.5 µl of 5× iScript No-RT Supermix was added.

cDNA samples were diluted to a working concentration of 5 ng/µl and qRT-PCR reactions were performed with the SsoAdvanced SYBR Green Supermix (Bio-Rad, 172-5261) using a CFX96 Thermal Cycler (Bio-Rad) following the manufacturer's suggested protocol. NRT and no template control (NTC) samples were included for each gene target.

Primer set pairs used in these studies are listed in Table S8. Prior to use for quantitating transcripts, primer pair efficiency was tested on six standard controls (serial dilutions of 1/5): 25 ng=2.50E+04, 5 ng=5.00E+03, 1 ng=1.00E+03, 0.2 ng=2.00E+02, 0.04 ng=4.00E+01 and 0.008 ng=8.00E+00. For statistical analysis, means were compared by one-way ANOVA followed by Tukey post-hoc analyses.

Glutaraldehyde vibratome sections

Following ISH, embryos were selected for sectioning. Sectioning was performed as previously described (Young et al., 2014). Briefly, embryos were equilibrated in a PBS solution containing 20% sucrose, 30% BSA and 4.9% gelatin, and fixed with 1.5% glutaraldehyde. Embryos were mounted into a Peel-A-Way disposable embedding mold (Polysciences, 18985). Once cured, the blocks were removed from the embedding molds and cut into sectioning prisms using a razor blade. Prisms were affixed to Heroscape dice (Hasbro) with super glue, mounted on a Pelco 101 Vibratome Series 1000 Sectioning System (Ted Pella) and cut into 50-75 µm sections using razor blades (Personna). The sections were mounted on glass slides for imaging using ProLong Gold antifade reagent (P36934) and a coverslip.

Microinjection of CRISPR/cas9: Zygotic *taf15* depletion

X. tropicalis taf15 sgRNA was designed using the Giraldez Lab CRISPRscan (crisprscan.org). Sequence of *X. tropicalis taf15* sgRNA (including the protospacer adjacent motif, underlined): GCTATGGTGGTTATGGAG-GAGG. sgRNA was generated by PCR amplification using the Phusion DNA Polymerase (New England Biolabs, M0530S) following the manufacturer's protocol.

Forward primer: CTAGCTAATACGACTCACTATAGGCTATGGTGG-TTATGGAGGGTTTTAGAGCTAGAA; reverse primer: AAAAGCACC-GACTCGGTGCCACTTTTTCAAGTTGATAACGGACTAGCCTTATTT-TAACTTGCTATTTCTAGCTCTAAAC were used for sgRNA amplification. RNA *in vitro* transcription of sgRNA was performed using the T7 MEGAshortscript kit (Ambion/Life Technologies, AM1354) and sgRNA clean-up was performed using the MEGAclear kit (Ambion/Life Technologies, AM1908).

sgRNA injection cocktails included 1.5 ng Cas9 protein, 400 ng sgRNA and Dextran555 (Life Technologies/Molecular Probes, D34679) diluted in water. The injection volume was 2 nl. Embryos were injected at the two-cell

stage, into either one or both cells, to deplete target mRNA from half or the whole embryo, respectively.

Acknowledgements
We thank Marta Truchado Garcia and Edivinia Pangilinan of the Harland lab at the University of California, Berkeley for organizing reagents for revision experiments. We also thank Helen Willsey of Matthew State's lab for providing *X. tropicalis* embryos for revision experiments. We thank Jim Boonyaratanakornkit and Matthew Gray of Justin Taylor's lab at the Fred Hutchinson Cancer Research Center for their time and western blot reagents used for revision experiments.

Competing interests
The authors declare no competing or financial interests.

Author contributions
Conceptualization: C.S.D., R.M.H.; Methodology: C.S.D., D.S.D.; Software: D.S.D.; Validation: C.S.D., C.R.T.E., Y.X.; Formal analysis: C.S.D., D.S.D.; Investigation: C.S.D.; Resources: R.M.H.; Data curation: D.S.D.; Writing - original draft: C.S.D.; Writing - review & editing: R.M.H.; Visualization: C.S.D.; Funding acquisition: R.M.H.

Funding
This work was supported by the National Institutes of Health (R01GM42314 and R35GM127069 to R.M.H.). C.R.T.E. and Y.X. were supported by the National Institute of Mental Health (U01MH115747) and a gift from the Overlook International Foundation to Matthew State (UCSF). Deposited in PMC for release after 12 months.

Data availability
RNA-seq data have been deposited in Gene Expression Omnibus under accession number GSE180671.

Peer review history
The peer review history is available online at https://journals.biologists.com/dev/article-lookup/doi/10.1242/dev.191619

References

Alves, J., Wurdak, H., Garay-Malpartida, H. M., Harris, J. L., Occhiucci, J. M., Belizário, J. E. and Li, J. (2009). TAF15 and the leukemia-associated fusion protein TAF15-CIZ/NMP4 are cleaved by caspases-3 and -7. *Biochem. Biophys. Res. Commun.* **384**, 495-500. doi:10.1016/j.bbrc.2009.05.009

Andersson, M. K., Ståhlberg, A., Arvidsson, Y., Olofsson, A., Semb, H., Stenman, G., Nilsson, O. and Åman, P. (2008). The multifunctional FUS, EWS and TAF15 proto-oncoproteins show cell type-specific expression patterns and involvement in cell spreading and stress response. *BMC Cell Biol.* **9**, 37. doi:10.1186/1471-2121-9-37

Ballarino, M., Jobert, L., Dembélé, D., de la Grange, P., Auboeuf, D. and Tora, L. (2013). TAF15 is important for cellular proliferation and regulates the expression of a subset of cell cycle genes through miRNAs. *Oncogene* **32**, 4646-4655. doi:10.1038/onc.2012.490

Black, D. L. (2003). Mechanisms of alternative pre-messenger RNA splicing. *Annu. Rev. Biochem.* **72**, 291-336. doi:10.1146/annurev.biochem.72.121801.161720

Boutz, P. L., Bhutkar, A. and Sharp, P. A. (2015). Detained introns are a novel, widespread class of post-transcriptionally spliced introns. *Genes Dev.* **29**, 63-80. doi:10.1101/gad.247361.114

Crozat, A., Åman, P., Mandahl, N. and Ron, D. (1993). Fusion of CHOP to a novel RNA-binding protein in human myxoid liposarcoma. *Nature* **363**, 640-644. doi:10.1038/363640a0

Delattre, O., Zucman, J., Plougastel, B., Desmaze, C., Melot, T., Peter, M., Kovar, H., Joubert, I., de Jong, P., Rouleau, G. et al. (1992). Gene fusion with an ETS DNA-binding domain caused by chromosome translocation in human tumours. *Nature* **359**, 162-165. doi:10.1038/359162a0

Dichmann, D. S. and Harland, R. M. (2012). fus/TLS orchestrates splicing of developmental regulators during gastrulation. *Genes Dev.* **26**, 1351-1363. doi:10.1101/gad.187278.112

Dichmann, D. S., Fletcher, R. B. and Harland, R. M. (2008). Expression cloning in *Xenopus* identifies RNA-binding proteins as regulators of embryogenesis and Rbmx as necessary for neural and muscle development. *Dev. Dyn.* **237**, 1755-1766. doi:10.1002/dvdy.21590

Grabowski, P. J. and Black, D. L. (2001). Alternative RNA splicing in the nervous system. *Prog. Neurobiol.* **65**, 289-308. doi:10.1016/S0301-0082(01)00007-7

Gregory, R. I., Yan, K.-P., Amuthan, G., Chendrimada, T., Doratotaj, B., Cooch, N. and Shiekhattar, R. (2004). The Microprocessor complex mediates the genesis of microRNAs. *Nature* **432**, 235-240. doi:10.1038/nature03120

Heasman, J., Crawford, A., Goldstone, K., Garner-Hamrick, P., Gumbiner, B., McCrea, P., Kintner, C. and Noro, C. Y. and Wylie, C. (1994). Overexpression of cadherins and underexpression of ?-catenin inhibit dorsal mesoderm induction in early Xenopus embryos. *Cell* **79**, 791-803. doi:10.1016/0092-8674(94)90069-8

Heasman, J., Kofron, M. and Wylie, C. (2000). βCatenin signaling activity dissected in the early xenopus embryo: a novel antisense approach. *Dev. Biol.* **222**, 124-134. doi:10.1006/dbio.2000.9720

Hicks, G. G., Singh, N., Nashabi, A., Mai, S., Bozek, G., Klewes, L., Arapovic, D., White, E. K., Koury, M. J., Oltz, E. M. et al. (2000). Fus deficiency in mice results in defective B-lymphocyte development and activation, high levels of chromosomal instability and perinatal death. *Nat. Genet.* **24**, 175-179. doi:10.1038/72842

Hoell, J. I., Larsson, E., Runge, S., Nusbaum, J. D., Duggimpudi, S., Farazi, T. A., Hafner, M., Borkhardt, A., Sander, C. and Tuschl, T. (2011). RNA targets of wild-type and mutant FET family proteins. *Nat. Struct. Mol. Biol.* **18**, 1428-1431. doi:10.1038/nsmb.2163

Hongo, I., Kengaku, M. and Okamoto, H. (1999). FGF signaling and the anterior neural induction in Xenopus. *Dev. Biol.* **216**, 561-581. doi:10.1006/dbio.1999.9515

Imai, Y., Gates, M. A., Melby, A. E., Kimelman, D., Schier, A. F. and Talbot, W. S. (2001). The homeobox genes vox and vent are redundant repressors of dorsal fates in zebrafish. *Development* **128**, 2407-2420. doi:10.1242/dev.128.12.2407

Iwasaki, Y. and Thomsen, G. H. (2014). The splicing factor PQBP1 regulates mesodermal and neural development through FGF signaling. *Development* **141**, 3740-3751. doi:10.1242/dev.106658

Kapeli, K., Pratt, G. A., Vu, A. Q., Hutt, K. R., Martinez, F. J., Sundararaman, B., Batra, R., Freese, P., Lambert, N. J., Huelga, S. C. et al. (2016). Distinct and shared functions of ALS-associated proteins TDP-43, FUS and TAF15 revealed by multisystem analyses. *Nat. Commun.* **7**, 12143. doi:10.1038/ncomms12143

Kato, M., Han, T. W., Xie, S., Shi, K., Du, X., Wu, L. C., Mirzaei, H., Goldsmith, E. J., Longgood, J., Pei, J. et al. (2012). Cell-free formation of RNA granules: low complexity sequence domains form dynamic fibers within hydrogels. *Cell* **149**, 753-767. doi:10.1016/j.cell.2012.04.017

Khokha, M. K., Chung, C., Bustamante, E. L., Gaw, L. W. K., Trott, K. A., Yeh, J., Lim, N., Lin, J. C. Y., Taverner, N., Amaya, E. et al. (2002). Techniques and probes for the study of Xenopus tropicalis development. *Dev. Dyn.* **225**, 499-510. doi:10.1002/dvdy.10184

Khokha, M. K., Yeh, J., Grammer, T. C. and Harland, R. M. (2005). Depletion of three BMP antagonists from Spemann's organizer leads to a catastrophic loss of dorsal structures. *Dev. Cell* **8**, 401-411. doi:10.1016/j.devcel.2005.01.013

King, O. D., Gitler, A. D. and Shorter, J. (2012). The tip of the iceberg: RNA-binding proteins with prion-like domains in neurodegenerative disease. *Brain Res.* **1462**, 61-80. doi:10.1016/j.brainres.2012.01.016

Kovar, H. (2011). Dr. Jekyll and Mr. Hyde: the two faces of the FUS/EWS/TAF15 protein family. *Sarcoma* **2011**, 837474. doi:10.1155/2011/837474

Li, H., Watford, W., Li, C., Parmelee, A., Bryant, M. A., Deng, C., O'Shea, J. and Lee, S. B. (2007). Ewing sarcoma gene EWS is essential for meiosis and B lymphocyte development. *J. Clin. Investig.* **117**, 1314-1323. doi:10.1172/JCI31222

Liu, Z., Scannell, D. R., Eisen, M. B. and Tjian, R. (2011). Control of embryonic stem cell lineage commitment by core promoter factor, TAF3. *Cell* **146**, 720-731. doi:10.1016/j.cell.2011.08.005

Love, M. I., Huber, W. and Anders, S. (2014). Moderated estimation of fold change and dispersion for RNA-seq data with DESeq2. *Genome Biol.* **15**, 550. doi:10.1186/s13059-014-0550-8

Martini, A., La Starza, R., Janssen, H., Corveleyn, A., Somers, R., Aventin, A. and Marynen, P. (2002). Advances in brief recurrent rearrangement of the Ewing ' s sarcoma gene, EWSR1, or its homologue, TAF15, with the transcription factor CIZ/NMP4 in Acute Leukemia. *Cancer* **1**, 5408-5412.

Mitros, T., Lyons, J. B., Session, A. M., Jenkins, J., Shu, S., Kwon, T., Lane, M., Ng, C., Grammer, T. C., Khokha, M. K. et al. (2019). A chromosome-scale genome assembly and dense genetic map for Xenopus tropicalis. *Dev. Biol.* **452**, 8-20. doi:10.1016/j.ydbio.2019.03.015

Neumann, M., Bentmann, E., Dormann, D., Jawaid, A., DeJesus-Hernandez, M., Ansorge, O., Roeber, S., Kretzschmar, H. A., Munoz, D. G., Kusaka, H. et al. (2011). FET proteins TAF15 and EWS are selective markers that distinguish FTLD with FUS pathology from amyotrophic lateral sclerosis with FUS mutations. *Brain* **134**, 2595-2609. doi:10.1093/brain/awr201

Nieuwkoop, P. D. and Faber, J. (1994). *Normal Table of Xenopus Laevis (Daudin): A System- Atical and Chronological Survey of the Development from the Fertilized Egg Till the end of Metamorphosis*. New York: Garland Publishing.

Ninomiya, K., Kataoka, N. and Hagiwara, M. (2011). Stress-responsive maturation of Clk1/4 pre-mRNAs promotes phosphorylation of SR splicing factor. *J. Cell Biol.* **195**, 27-40. doi:10.1083/jcb.201107093

Onichtchouk, D., Glinka, A. and Niehrs, C. (1998). Requirement for Xvent-1 and Xvent-2 gene function in dorsoventral patterning of Xenopus mesoderm. *Development* **125**, 1447-1456. doi:10.1242/dev.125.8.1447

Panagopoulos, I., Mencinger, M., Dietrich, C. U., Bjerkehagen, B., Saeter, G., Mertens, F., Mandahl, N. and Heim, S. (1999). Fusion of the RBP56 and CHN genes in extraskeletal myxoid chondrosarcomas with translocation t(9;17)(q22;q11). *Oncogene* **18**, 7594-7598. doi:10.1038/sj.onc.1203155

Pandya-Jones, A. (2011). Pre-mRNA splicing during transcription in the mammalian system. *Wiley Interdiscip. Rev. RNA* **2**, 700-717. doi:10.1002/wrna.86

Pandya-Jones, A. and Black, D. L. (2009). Co-transcriptional splicing of constitutive and alternative exons. *RNA* **15**, 1896-1908. doi:10.1261/rna.1714509
Perales, R. and Bentley, D. (2009). 'Cotranscriptionality': the transcription elongation complex as a nexus for nuclear transactions. *Mol. Cell* **36**, 178-191. doi:10.1016/j.molcel.2009.09.018
Rabbitts, T. H., Forster, A., Larson, R. and Nathan, P. (1993). Fusion of the dominant negative transcription regulator CHOP with a novel gene FUS by translocation t(12;16) in malignant liposarcoma. *Nat. Genet.* **4**, 175-180. doi:10.1038/ng0693-175
Rawat, V. P. S., Arseni, N., Ahmed, F., Mulaw, M. A., Thoene, S., Heilmeier, B., Sadlon, T., D'Andrea, R. J., Hiddemann, W., Bohlander, S. K. et al. (2010). The vent-like homeobox gene VENTX promotes human myeloid differentiation and is highly expressed in acute myeloid leukemia. *Proc. Natl. Acad. Sci. USA* **107**, 16946-16951. doi:10.1073/pnas.1001878107
Reversade, B., Kurado, H. and Lee, H., Mays, A. and De Robertis, E. M. (2005). Depletion of Bmp2, Bmp4, Bmp7 and Spemann organizer signals induces massive brain formation in Xenopus embryos. *Development* **132**, 3381-3392. doi:10.1242/dev.01901
Reyes, A., Anders, S. and Huber, W. (2014). *Inferring Differential Exon Usage in RNA-Seq Data with the DEXSeq Package*, Heidelberg, Germany: EMBL.
Sander, V., Reversade, B. and De Robertis, E. M. (2007). The opposing homeobox genes Goosecoid and Vent1/2 self-regulate Xenopus patterning. *EMBO J.* **26**, 2955-2965. doi:10.1038/sj.emboj.7601705
Scekic-Zahirovic, J., Sendscheid, O., El Oussini, H., Jambeau, M., Sun, Y., Mersmann, S., Wagner, M., Dieterlé, S., Sinniger, J., Dirrig-Grosch, S. et al. (2016). Toxic gain of function from mutant FUS protein is crucial to trigger cell autonomous motor neuron loss. *EMBO J.* **35**, 1077-1097. doi:10.15252/embj.201592559
Schuler-Metz, A., Knöchel, S., Kaufmann, E. and Knöchel, W. (2000). The homeodomain transcription factor Xvent-2 mediates autocatalytic regulation of BMP-4 expression in *Xenopus*embryos. *J. Biol. Chem.* **275**, 34365-34374. doi:10.1074/jbc.M003915200
Schwartz, J. C., Wang, X., Podell, E. R. and Cech, T. R. (2013). RNA seeds higher-order assembly of FUS protein. *Cell Rep.* **5**, 918-925. doi:10.1016/j.celrep.2013.11.017
Schwartz, J. C., Cech, T. R. and Parker, R. R. (2015). Biochemical Properties and Biological Functions of FET Proteins. *Annu. Rev. Biochem.* **84**, 355-379. doi:10.1146/annurev-biochem-060614-034325
Sharma, A., Lyashchenko, A. K., Lu, L., Nasrabady, S. E., Elmaleh, M., Mendelsohn, M., Nemes, A., Tapia, J. C., Mentis, G. Z. and Shneider, N. A. (2016). ALS-associated mutant FUS induces selective motor neuron degeneration through toxic gain of function. *Nat. Commun.* **7**, 10465. doi:10.1038/ncomms10465
Shiohama, A., Sasaki, T., Noda, S., Minoshima, S. and Shimizu, N. (2007). Nucleolar localization of DGCR8 and identification of eleven DGCR8-associated proteins. *Exp. Cell Res.* **313**, 4196-4207. doi:10.1016/j.yexcr.2007.07.020
Sive, H. L., Grainger, R. M. and Harland, R. M. (2000). *Early Development of Xenopus Laevis. A Laboratory Manual*, Cold Spring Harbor, New York: Cold Spring Harbor Laboratory Press.
Sjögren, H., Meis-Kindblom, J., Kindblom, L. G., Åman, P. and Stenman, G. (1999). Fusion of the EWS-related gene TAF2N to TEC in extraskeletal myxoid chondrosarcoma. *Cancer Res.* **59**, 5064-5067.
Svetoni, F., Frisone, P. and Paronetto, M. P. (2016). Role of FET proteins in neurodegenerative disorders. *RNA Biol.* **13**, 1089-1102. doi:10.1080/15476286.2016.1211225
Tan, A. Y. and Manley, J. L. (2009). The TET family of proteins: functions and roles in disease. *J. Mol. Cell Biol.* **1**, 82-92. doi:10.1093/jmcb/mjp025
Trapnell, C., Roberts, A., Goff, L., Pertea, G., Kim, D., Kelley, D. R., Pimentel, H., Salzberg, S. L., Rinn, J. L. and Pachter, L. (2012). Differential gene and transcript expression analysis of RNA-seq experiments with TopHat and Cufflinks. *Nat. Protoc.* **7**, 562-578. doi:10.1038/nprot.2012.016
Vance, C., Rogelj, B., Hortobagyi, T., De Vos, K. J., Nishimura, A. L., Sreedharan, J., Hu, X., Smith, B., Ruddy, D., Wright, P. et al. (2009). Mutations in FUS, an RNA processing protein, cause familial amyotrophic lateral sclerosis Type 6. *Science* **323**, 1208-1211. doi:10.1126/science.1165942
Young, J. J., Kjolby, R. A. S., Kong, N. R., Monica, S. D. and Harland, R. M. (2014). Spalt-like 4 promotes posterior neural fates via repression of pou5f3 family members in Xenopus. *Development* **141**, 1683-1693. doi:10.1242/dev.099374